Nanostructured multilayer CAE-PVD coatings based on transition metal nitrides on Ti6Al4V alloy for biomedical applications

Nanostructured multilayer CAE-PVD coatings based on transition metal nitrides on Ti6Al4V alloy for biomedical applications

Mahdis Noori[a,b], Masoud Atapour[1a], Fakhreddin Ashrafizadeh[a], Hassan Elmkhah[c], Giovanna Gautier di Confiengo[d], Sara Ferraris[b], Sergio Perero[b], Marilena Cardu [b], Silvia Spriano[b]

[a] Department of Materials Engineering, Isfahan University of Technology, Isfahan, 84156-83111, Iran

[b] Department of Applied Science and Technology, Politecnico di Torino, 10129 Torino (TO), Italy

[c] Faculty of Engineering, Bu-Ali Sina University, Hamedan, 65178-38695, Iran

[d] CNR-STEMS, 10135 Torino (TO), Italy

Abstract

Titanium alloys possess poor resistance to friction and this adversely affects the corrosion behavior and osseointegration of the implants made from these alloys. Nanostructured PVD coatings with biocompatibility, anti-wear and anti-corrosion characteristics have attracted much attention in biomedical applications. In this study, TiN and ZrN single layer and CrN/TiN and CrN/ZrN nanostructured multilayer thin films were applied on a Ti6Al4V substrate by means of cathodic arc PVD technique. The physical-chemical characterization of the coatings was conducted using FE-SEM, EDS, and XRD analyses. Their surface topography and wettability were measured. In addition, the hardness and adhesion strength were evaluated by means of Knoop microhardness and scratch tests, respectively. Also, the apatite-forming ability of the coatings was investigated through SEM, EDS and, FTIR. The corrosion performance of the coatings was studied using PDP and EIS assessments in SBF solution. According to the findings, the multilayer coatings have higher hardness and scratch resistance than single layers. The coating delamination tacked place in L_c equal 39.6 (N) and 39.3 (N) for CrN/TiN and CrN/ZrN coatings, respectively. The corrosion assessments revealed that the CrN/ZrN multilayer coating exhibited the best corrosion resistance due to its smoother surface and more dense structure in addition to its specific architecture. The ZrN single layer and CrN/ZrN multilayer coatings showed a better hydroxyapatite precipitation; however, all surfaces had satisfactory bioactivity. In all, this study showed that CrN/ZrN nanostructured multilayer thin film is potentially suitable candidates for orthopedic and dental implants.

Keywords: Arc-PVD, Single layer, Multilayer coatings, CrN/TiN, CrN/ZrN.

1. Introduction

The high biocompatibility, high strength-to-weight ratio, and low elasticity module of titanium and its alloys caused them to be largely used in making medical implants [1]. The titanium oxide layer which is naturally created on the titanium/ titanium alloy surface is the main reason for the high corrosion resistance of these materials. However, this oxide film can be damaged if shear forces and micro-movements are applied to it because of the low friction resistance of titanium-

[1] Corresponding author; Tel. +983133915735; Fax +983133912752; Email: m.atapour@cc.iut.ac.ir

based biomaterials. As a result, harmful metallic ions and fine metallic debris can be released into the surrounding tissues causing the inflammatory cascade [2,3]. Even if the bone (dental or orthopaedic) implants made in titanium are not used for devices with macro movements under loading, several steps of the implant manufacturing and life can induce friction forces, micro-movements, or corrosive environments: cleaning and disinfection of the implant surface through mechanical, physical or chemical methods, implant insertion in the bone, presence of bone fragments in the surgical site, inflammatory response with acidic pH, fretting with the cement or with the bone before osteointegration, friction between the internal implant walls and the prosthetic abutment [4]. The deposition of a thin protective film with high hardness and friction resistance, on the titanium implants, can be a proper solution to these issues [5,6].

Among different protective coatings, thin films of transition metal nitrides, including those made of TiN [5,7], ZrN [2,8], CrN [9,10] and NbN [10,11], are welcomed by researchers because of their high hardness, stable friction behavior, high wear and corrosion resistance, and high chemical stability. Different methods have been used for the deposition of these materials. Among these methods, Cathodic Arc Evaporation Physical Vapor Deposition (CAE-PVD) is one of the most efficient physical vapor deposition methods that create dense coatings with high adhesion to the substrate [12]. However, the appearance of many microparticles followed by pinholes on the final surface of the coating is the most significant weak point of this method [13]. The excessive presence of pinholes in the coating has harmful effects on the performance of the coating in the corrosive media of the body, especially when subjected to sliding conditions and under micro-motions [14].

The development of nanostructured multilayers (superlattices) is a crucial approach for increasing the performance of the coatings created using the CAE-PVD method. Researchers have been interested in this strategy for several decades [14–17]. The interfaces in the multilayer structures serve as a barrier against the corrosive electrolytes of the body to path through the substrate. Additionally, the columnar structure of the coating is prevented by the deposition of alternating layers, limiting the electrolyte's passage to the substrate. With this approach, the achieved coatings have more protective properties against corrosion [18]. Their superior adhesion to the substrate, caused by the stress gradient distribution within them, and also their higher hardness and wear resistance, than single layers, make them more stable under sliding conditions [19].

Different attempts were made to evaluate the nitride-based single layer and multilayer coatings for various applications. For instance, CrN/MoN [20], CrN/ZrN [17,21,22], CrN/TiN [23,24] ,TiN/TaN [25,26] have been developed during recent years. It needs to note that most of these coatings were applied on steel-based substrates. Table 1 summarizes some of the published works focused on multilayer coatings and their properties. This literature survey shows that limited works are reported on nanostructured multilayer coatings on titanium-based alloys for biomedical applications. In recent years, TiAlN/TiN coating was fabricated on Ti45Nb substrate [27] and TiN/CrN coating was constructed on Ni/Ti substrate [28] and, Ti6Al4V [29] for biomedical applications but in a different form of nanolayers configuration and thickness, than our coatings.

According to our previous works[30,31] the layer architecture is an important factor influencing the mechanical properties and corrosion behavior of the multilayer PVD coatings. To the best of our knowledge, there are no reports available in the literature concerning the corrosion and bioactivity properties of nanolayered CrN/TiN and CrN/ZrN multilayer coatings. This study aimed to investigate the structure, corrosion resistance and bioactivity of two multilayer thin films on Ti6Al4V for biomedical applications. For this purpose, CrN/TiN and CrN/ZrN multilayer coatings with special layer architecture were fabricated on Ti6Al4V substrate using cathodic-arc evaporation (CAE) PVD process. For comparison aspects, TiN and ZrN single layers were also coated on Ti6Al4V. In order to obtain a better comparison, the same thickness of different coatings was applied to the Ti6Al4V substrate by adjusting the deposition parameters, the microstructure, surface characteristics, bioactivity, scratch and corrosion resistance of the prepared coatings have been carefully investigated.

Table 1. Some previous studies have been conducted on the properties of nanostructured multilayer coatings

Coating and deposition method	Substrate	Application	Thickness	Corrosion behavior(electrochemical tests)	Bioactivity	Scratch resistance	Ref
Annealed CrN/ CrAlN CAE-PVD	304 stainless steel	Industerial	N/A	Has been investigated by EIS in 3.5% NaCl. The maximum R_p is 32 MΩ for annealed CrN/CrAlN in 700°C.	N/A	N/A	[32]
TiN/CrN CAE-PVD	Carburized-H13 hot-work steel	Industrial	2 µm	Has been investigated by EIS in 3.5% NaCl. The maximum R_p is 3800 Ω for TiN/CrN	N/A	N/A	[33]
TiN/CrN CAE-PVD	Nickel-chromium dental alloy	Dental fixed prosthesis	1.8± 0.2 µm	Has been investigated by EIS in artificial saliva. The maximum R_p is 59440 and 356104 Ω for CrN/TiN in PH=3 and 6.5 respectively.	N/A	N/A	[28]
CrN/TiN CAE-PVD	Ti-6Al-4 V	Biomedical	~2 µm	Has been investigated by EIS in Hank's solution. The maximum R_p is 825560Ω for CrN/TiN.	N/A	N/A	[29]
ZrN/CrN CAE-PVD	AISI 304	Industrial	N/A	Has been investigated by EIS in 3.5% NaCl. The maximum R_p after 24h immersion is 1321990 Ω for ZrN/CrN.	N/A	N/A	[34]
CrN/TiN CAE-PVD	Ni–Cr ceramic dental alloys	Dental implant	1.8± 0.2 µm	Has been investigated in Hank's solution. The maximum R_p is 96292Ω for CrN/TiN.	N/A	N/A	[35]
CrN/ CrAlN and CrCN/CrAlCN CAE-PVD	430 Stainless Steel	Industrial	3.29 µm	Has been investigated by EIS in 3.5% NaCl. The maximum R_p is 145183Ω and 6396080 Ω for CrN/ CrAlN and CrCN/CrAlCN ,respectively(after 1 day immersion).	N/A	N/A	[36]
TiN/NbN Mixed HIPIMS-UBM*	CoCrMo alloy	Biomedical	3.95 µm	N/A	N/A	N/A	[11]
ZrN/CrN with 10 bilayers (10 L), 20 bilayers (20 L) and 30 bilayers (30 L) periodes CAE-PVD	AISI 304 stainless steel	Industrial	N/A	Has been investigated by EIS in 3.5% NaCl. The maximum R_p is 1.67×10^6, 6.94×10^6 and 10.41×10^6 Ω for ZrN/CrN with 10 L, 20 L and 30 L bilayers respectively(after 1 day immersion).	N/A	N/A	[37]
TiN/NbN DC reactive magnetron sputtering	316L Stainless Steel	Biomedical	1.6µm	Has been investigated by PDP analysis. The higher corrosion potential and lower corrosion current density is for TiN/NbN in comparison with single layers.	N/A	N/A	[38]
ZrN/CrN CAE-PVD	AISI 304 Stainless Steel	Industrial	N/A	Has been investigated in 3.5% NaCl. The maximum R_p is 1.32×10^6Ω for ZrN/CrN.	N/A	N/A	[21]
Zr/ZrN and TiN/ZrN CAE-PVD	TiNiNb alloy	Biomedical	~600 nm	Has been investigated by Tofel polarization tests in Ringer solution. The i_{corr} is 1.8×10^{-8}A for Zr/ZrN and 4.2×10^{-8}A for ZrN/TiN.	N/A	N/A	[39]
TiN/ TiAlSiN	TC18	Industrial	3.8 µm	N/A	N/A	The critical load for	[40]

Multi-arc ion plating technique	(Ti5Al5Mo5 V1CrFe) alloy					TiN/ TiAlSiN was up to 62.4 N	
ZrN/CrN CAE-PVD	AISI321 Stainless Steel	Industrial	628 nm	N/A	N/A	N/A	[22]
TiN/CrN UBM	tungsten carbide	Industrial	1.77 µm	N/A	N/A	The critical load was 24.7N and 45.1N for TiN single layer and TiN/CrN multilayer, respectively	[16]
TiN/TiCN DC magnetron sputtering	2520-310S steel	Industrial	23.5 µm	N/A	N/A	The critical load was 23.5 N for TiN/TiCN	[41]
* High Power Impulse Magnetron Sputtering-Unbalanced Magnetron Sputtering							

2. Experimental procedure

2.1. Coating fabrication

The TiN and ZrN single layer and CrN/TiN and CrN/ZrN nanostructured multilayer coatings were deposited on Ti6Al4V substrates using CAE-PVD (DS&Ca6α Yarnikan Saleh, Iran). A commercial plate of Ti6Al4V (50 × 30 cm) with the following composition (Ti = 89.71%, Al = 4.49%, V = 3.37%, other < 0.43%) was used as substrate. Before the coating process, samples were cut in 10 mm × 10 mm × 1 mm dimensions. All of the samples were grinded with SiC grinding papers up to 1200 grit and then washed in an ultra-sonic cleaner once with ethanol and once with distilled water. The samples were then dried at room temperature. The samples were stored in the desiccator up to the start of the coating process in order to prevent any contamination.

After placing the samples in the coating chamber, the samples were under Ar^+ ion bombardment at 800 V for 10 minutes, in order to increase the coating adhesion strength. During the deposition process, very pure N_2 gas (99.96%) was introduced into the chamber. The targets below were used as a vacuum-arc set: Ti target (99.96%) for TiN single layer coating, Zr target (99.96%) for ZrN single layer coating, Ti and Cr (99.96%) targets for CrN/TiN nanostructured multilayer coating and Zr and Cr targets for CrN/ZrN nanostructured multilayer coating.

Coating parameters are mentioned in Table 2 in detail. For the deposition of multilayer coatings, the rotating stage holder of samples was stopped in specific time intervals to the cathodic bombardment of the samples for a specified period of time (predetermined time). The time was set up so that equal thickness of alternative layers of CrN/TiN and CrN/ZrN formed.

Table 2. Coating parameters

Coating Parameters	
Working pressure (Pa)	0.66
Current of target evaporation (A)	100
Deposition time (min)	90
Substrate rotating rate (rpm)	3
Deposition temperature (°C)	250
Substrate bias voltage (V)	-100
Substrate- target distance (mm)	150
Duty cycle (%)	50

2.2. Microstructure and surface characterization

For identifying the phase structure of the coatings and substrate the small angle X-ray diffraction analysis (XRD, PANalytical X'Pert Pro PW 3040160 Philips, Malvern Panalytical, Egham, United Kingdom) was used. This analysis has been done by using a pan-analytical X-ray diffractometer with Cu-kα radiation source with 1.54 A° wavelength and 0.001° step size in the 2θ scan range from 20 to 80 in θ - 2θ Bragg-Brentano mode. The Philips Xpert high score™ and Origin™ software were used for data elaboration. The JCPDS database has been used for the identification of the phases (JCPDS sheet no. 044-1294 has been used for the Ti α phase and no. 044-1288 for the β phase; no. 038-1420 for TiN; no. 076-2494 for CrN and no. 035-0803 for Cr_2N; no. 074-1217 for ZrN).
Morphological characterization of coated samples was done by Field Emission Scanning Electron Microscopy (FE-SEM, MIRA3-XMU, Czech). To estimate the coating composition, energy-dispersive X-Ray spectrometry (EDX, Seron AIS 2300™) was used. For evaluating the cross-section of coatings and measuring the thickness of them, the samples, mounted in phenolic resin, were grinded with SiC grinding papers up to 2500 grit. After that, the samples were polished via polishing clothes using an alumina powder with a size of 0.05 µm. In the next step, the surfaces were washed with distilled water, and then they were cooled down in the warm airflow.

The roughness of the substrate and coated samples was quantified by means of a contact profiler equipped with a diamond stylus tip (Taylor-Hobson, Form Talysurf 120L™, UK). Each measurement was repeated 3 times. The data were elaborated with Taylymap™ software. Roughness parameters were determined by using ISO 25178 standard.

Hydrophobicity or hydrophilicity behavior of the raw and coated samples was determined by using the static contact angle analysis (Sessile drop method, DSA-100, KRUSS™, Gmbh Hamburg, Germany). Distilled water (5µL) was used as wetting fluid at room temperature. The measurement was repeated 5 times for each sample. Before the analysis, the samples were cleaned for ten minutes in an ethanol ultrasonic bath, followed by five minutes in distilled water, and then dried in a warm airflow.

The microhardness of samples was measured by a HV-1000 Knoop hardness tester (BIUGED™, Guangzhou, China) in a loading process at force 25 g and 15 seconds duration. 5 indentations were conducted for each sample and the results were averaged.

To evaluate the adhesion strength of coatings to the substrate, the scratch test was done in the Revetest mode (CSM^{TM} Revetest Machine, Anton Paar, Austria). The loading was done by using a Rockwell C diamond indenter with a 200 μm tip radius. Loading was progressively increased from 1 N to 50 N at the rate of 100 N/min, and the indenter speed was 100 mm/min. The scratch overall length was 4.99 mm. 5 scratches were made on each sample and the final result was obtained from their average. Applied load, friction coefficient, and Acoustic Emission (A.E.) signals were recorded continuously. In this analysis, the critical load (L_c) or the load at which the delamination of the coating begins is an index of the adhesion strength of the coating. A.E signal variations and optical observations of the scratch tracks were used to estimate this load. Scratched surfaces were examined with a scanning electron microscope (Jeol Jsm- 6490LV™, Japan) in order to have a precise investigation of the scratch morphology.

2.3. Bioactivity investigations

To investigate hydroxyapatite formation on the surface (bioactivity) of the fabricated coatings, the specimens were immersed in 50 mL simulated body fluid (SBF) and incubated at 37 ˚C for 14 days in a static condition in an incubator. The specimens were then removed from the SBF, rinsed with distilled water, and dried. The surface morphology and composition were investigated using SEM and EDS analyses. The SBF was prepared by dissolving some chemical material in distilled water. Then was buffered with $(CH_2OH)_3CNH_2$ and HCl in PH=7.4 and 37°C. The composition of SBF is depicted in Table 3. The formation of hydroxyapatite was identified using Fourier Transform Infrared analysis Spectroscopy (FTIR alpha Bruker optics, Ettlingen, Germany) after 14 days immersion.

Table 3. Chemical composition of SBF [42]

Material	Amount in 1000 ml of distilled water(gr)
Sodium chloride (NaCl)	8.035
Sodium hydrogen carbonate ($NaHCO_3$)	0.355
Potassium chloride (KCl)	0.225
Di-potassium hydrogen phosphate trihydrate ($K_2HPO_4.3H_2O$)	0.231
Magnesium chloride hexahydrate ($MgCl_2.6H_2O$)	0.311
Calcium chloride ($CaCl_2$)	0.290
Sodium sulfate (Na_2SO_4)	0.072
Tris-hydroxymethyl aminomethane ($(CH_2OH)_3CNH_2$)	6.118
Hydrochloric Acid (HCl) (1 M)	0-5 ml

2.4. Corrosion studies

The corrosion behavior of samples was studied by employing a potentiostat/galvanostat (AMETEK model PARSTAT 2273™, USA) in SBF at 37 ℃. The Potentiodynamic Polarization (PDP) test was done in the range from –0.25 V less than the open circuit potential (OCP) to 0.6 V at the 1 mv/s scan rate. The test was done in a 3 electrodes electrochemical cell containing a platinum plate, as a counter electrode, an Ag/AgCl (in saturated KCl solution), as a reference

electrode, and the raw substrate or coated samples, as the working electrode. PDP analysis was performed on 3 samples of raw substrate and each coating, and the findings with average amounts were presented. The samples were immersed in the electrolyte for 30 minutes before each test to achieve a steady state. The test results were analyzed using Powersuite software. Additionally the electrochemical impedance spectroscopy (EIS) measurements were carried out at OCP conditions with a step rate of 15 point/decade in the applied frequency range of 100 KHz to 10 MHz. Analysis was performed on 3 samples of each condition (uncoated and coated samples) and the results were fitted by means of Zview software.

3. Results and discussion

3.1 Crystallographic analysis

The XRD patterns of the substrate and single layers along with the nanostructured multilayer coatings are presented in Figure 1. The XRD spectrum of the CrN single layer is shown for a better understanding of the multilayer coatings' diffraction patterns. According to the spectrum of Ti6Al4V, α and β phases of Ti cannot be separately identified because of the overlapped diffraction reflections [43]. More than one diffraction reflection has been found on all coated samples, proving that the coatings are polycrystalline.

According to the diffraction pattern obtained on the CrN/TiN nanostructured multilayer coating, a TiN layer, with a Face Centered Cubic (fcc) structure, was recognized by the intense peaks placed at 2θ equal to 36.3° (111), 43.46° (200), 61.54° (220), 74.17° (311), and 77.71° (222), respectively. Also a Cr_xN layer, consisting of CrN (planes (111), (200), (220)) and the Cr_2N hexagonal phase, including the planes (002) and (111), was detected in this spectrum with lower intensity [16].

Additionally, it was observed that the XRD spectrum of the CrN/ZrN nanostructured multilayer coating includes intense peaks of the fcc phase ZrN ((111), (200), (220), (311), (222) planes), and weak diffraction signals of CrN (111), (200), (220) and Cr_2N (111) planes. These findings are in accordance with those of other researchers [22,44].

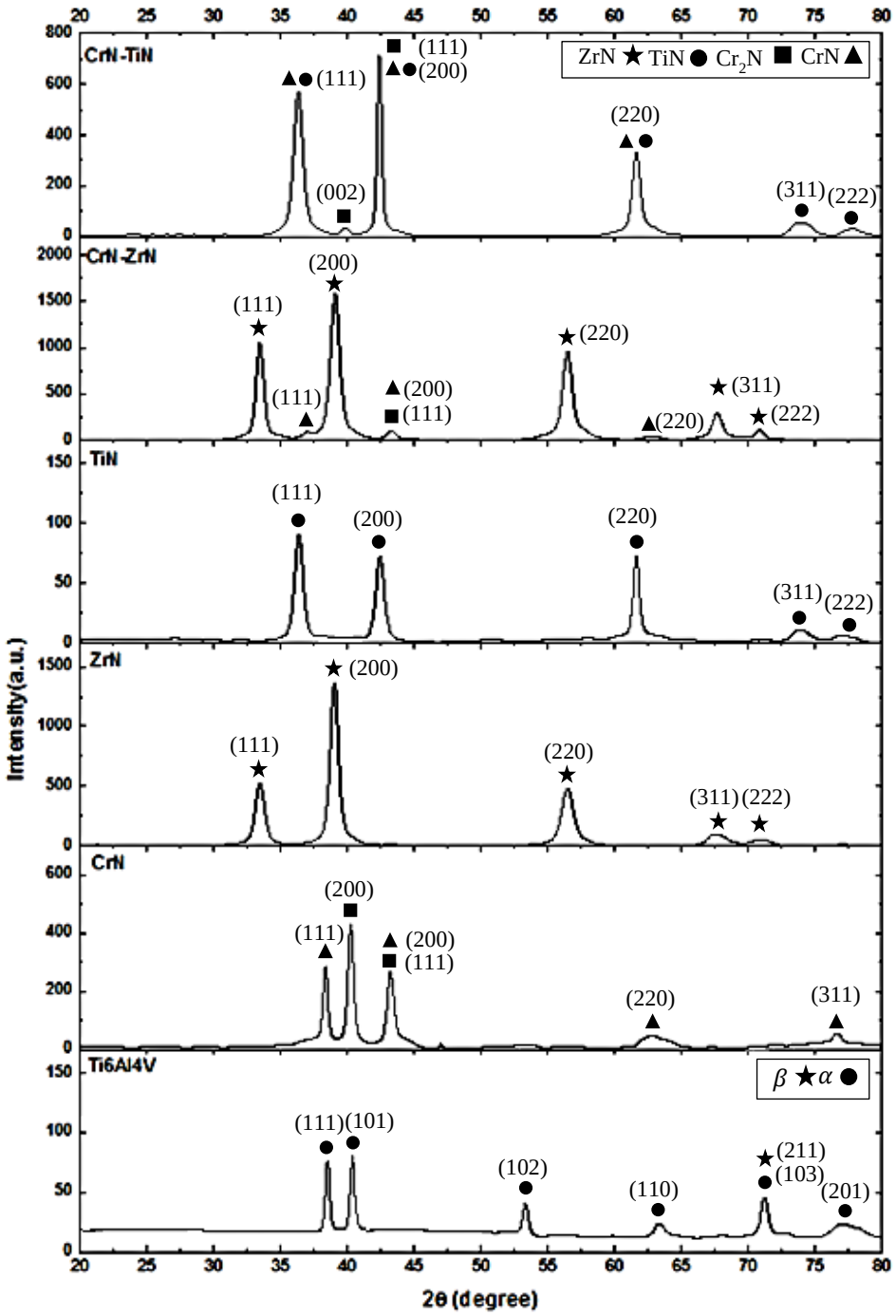

Figure 1 XRD patterns of the coated Ti6Al4V with CrN, TiN, ZrN single layers and CrN/TiN and CrN/ZrN nanostructured multilayer coatings.

3.2 Morphological and chemical characterization

In Figure 2, the top-surface FESEM images of single-layer and multilayer coatings are reported. As it can be seen in the images, all the coatings have microparticles on their surface (yellow arrows). It is unavoidable that these microparticles will form throughout the arc deposition process. Actuality, this phenomenon is one of the intrinsic features of the arc deposition process

[45]. These microparticles, mostly contain metallic phases as proven in some studies [46,47]. According to the study of Rujin Tian and his coworkers, the microparticles generated on the TiN coated surface are mostly titanium with a small amount of nitrogen [47]. The presence of nitrogen in the composition of these microparticles is inevitable because of the atmosphere of the deposition chamber. Therefore, the microparticles on the TiN coating surface are a solid solution of nitrogen in titanium, while the solid solution of nitrogen in chromium is for CrN coatings [46]. It is possible to regulate the density and size of the microparticles by adjusting the N_2 pressure, negative bias voltage, and target electric current. Additionally, they may be adjusted by utilizing a filtration system in the chamber [48]. These microparticles are easily removed from the surface because they have a weak bond with the matrix of the coating. The surface defects known as pinholes are caused by the detachment of these splattered microparticles from the surface [44], [48]. Even though these microparticles and pinholes can be seen in all of the coatings (red arrows), it is clear that they are different in number and size. It is noteworthy that, coating composition influences the density and size of these defects as proven in other studies. In this work, the ZrN single layer and CrN/ZrN nanostructured multilayer coatings are relatively smoother and more compact and homogenous than the TiN single layer and CrN/TiN nanostructured multilayer coatings. Actually, the density of microparticles and size of the pinholes on them are less than the two others. The reason is that the melting point of Zr is higher than that of Ti. It is crucial to understand that the melting and boiling points of the target have a significant impact on the final quality of coatings made using the arc process [46,49]. It is expected that the surface of the TiN single layer and CrN/TiN nanostructured multilayer coatings have more and bigger microparticles and pinholes than the two other coatings. These findings concur with those of previous research [49].

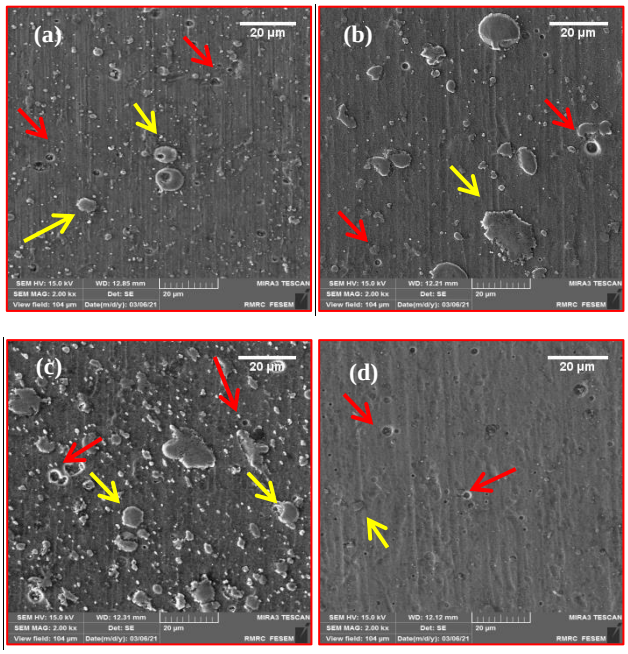

Figure 2 FE-SEM surface morphologies of (a) TiN; (b) ZrN single layers coatings; (c) CrN/TiN and (d) CrN/ZrN nanostructured multilayer coatings.

Cross-sectional microscopic micrographs of CrN/TiN and CrN/ZrN nanostructured multilayer coatings are shown in Figure 3 together with TiN and ZrN single layers. The architecture of nanostructured multilayer coatings is clearly defined in the highest magnified images. The observations imply that the coatings have a compact and dense morphology. There are no defects or internal cavities in the coating thickness. In all samples, the interface of the coating and substrate is free of any defect and exfoliation. This guarantees the high-quality adhesion of the coating to the substrate. These findings are in line with what has been proven in earlier investigations [17,50].

The use of an interlayer during the arc process is an appropriate technique which is employed for ensuring that the coating has good adhesion to the substrate. For TiN and ZrN single layers, thin layers of titanium and zirconium were deposited on the Ti6Al4V substrate, respectively, with a thickness of less than 100 nanometers. After that, the uniform, soft, and dense layers of TiN and ZrN were deposited on the mentioned interlayers respectively, with thicknesses of about 3 μm.

The design and architecture of multilayer coatings are different from those of single layers, nevertheless; that is why the coating parameters were set so that the overall thickness of all coatings would be equal. According to Figure 3 (c) and (d), which are related to the CrN/ZrN nanostructured multilayer coating, a Cr layer (thickness of less than 100 nm) and then a CrN layer (thickness of less than 0.8 μm) have been deposited as interlayers. The Cr layer guarantees the adhesion of the CrN layer to the substrate, as the CrN layer does for the upper layers. After the deposition of these two interlayers, the CrN and ZrN layers were deposited alternately, till the thickness of this region reached ≈ 1.75 μm. After that, a uniform monolayer of ZrN was deposited, on the top of the previous section containing alternating layers, with a ≈ 400 nm thickness. Because of the low temperature during the coating process (200 °C), penetration of the individual layers into each other could be ignored and that is why the nanolayers are observed with a clear interface and borders. The layers in this coating are visible as dark and bright tones due to differences in the electronic densities of the materials. Light gray layers are related to ZrN (with a thickness of about 50.07 nm) and the dark gray color is related to the CrN layer (with a thickness of about 64.20 nm). The CrN layers are thicker than the ZrN layers. Possible causes include the target current and the difference in the melting points of Cr and Zr. In this circumstance, the target with the highest current has the highest inlet energy, allowing deposition happens at a higher rate [51].

This approach is also used for the deposition of CrN/TiN nanostructured multilayer coating, but the difference is the deposition of TiN and CrN layers instead of ZrN and CrN. So, a new area with a thickness of about 1.8 μm was formed. Then a ≈ 500 nm uniform and soft layer of TiN was deposited as the last part. CrN and TiN layers are paired as darker and lighter layers. However, the layer contrast is not as strong as the CrN/ZrN coating. This is caused by the fact that the difference in electrical density of Cr and Ti is smaller than that between Cr and Zr. However, both coatings have uniform layers adhering to the substrate, creating a compact and dense structure. The wavy state of the interface between the layers is because of surface roughness which is caused by the splatting of microparticles on the surface [21].

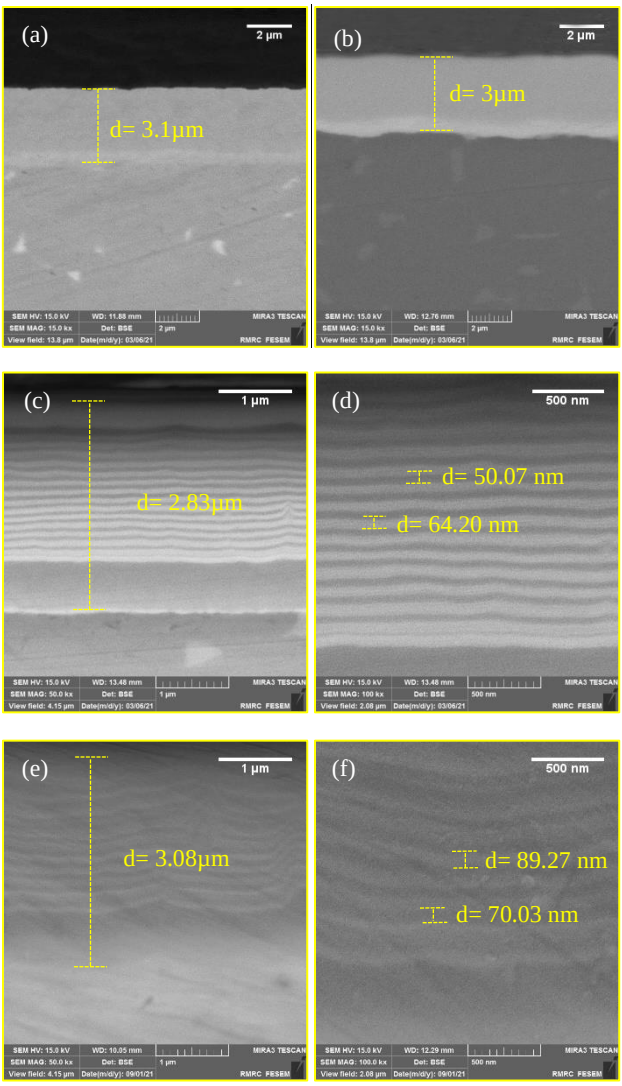

Figure 3 Cross-sectional FE-SEM images of (a) TiN; (b) ZrN single layers coatings; (c,d) CrN/ZrN and (e,f) CrN/TiN nanostructured multilayer coatings (in two magnifications).

The cross-sectional EDX-elemental line scans and maps of all the samples are presented in Figure 4-Figure 7. The line scan EDX profile of all the coatings demonstrates that the amount of the coating elements is substantial and extends to the depth of 3 µm. By coming closer to the interface of the substrate and coating, their amounts become lower and the amount of the substrate elements, especially Ti increases.

For those two multilayer coatings, the amount of their elements is presented as an approximation. The main reason is that the penetration depth in the EDX analysis is larger than the individual layer thickness. However, this condition is a little different in the case of N and it is obvious that it has a more uniform distribution than others. This procedure is proven in the cross-sectional elemental distribution map of coatings and it is easily comprehensible with the color separation done in the Figure 4-7.

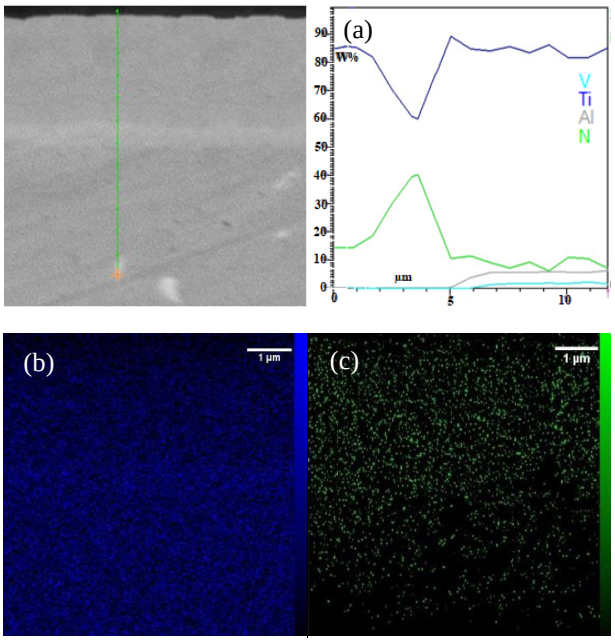

Figure 4 Cross-sectional EDS (a) line scan; (b) Ti and (c) N, map analysis of TiN single layer coating.

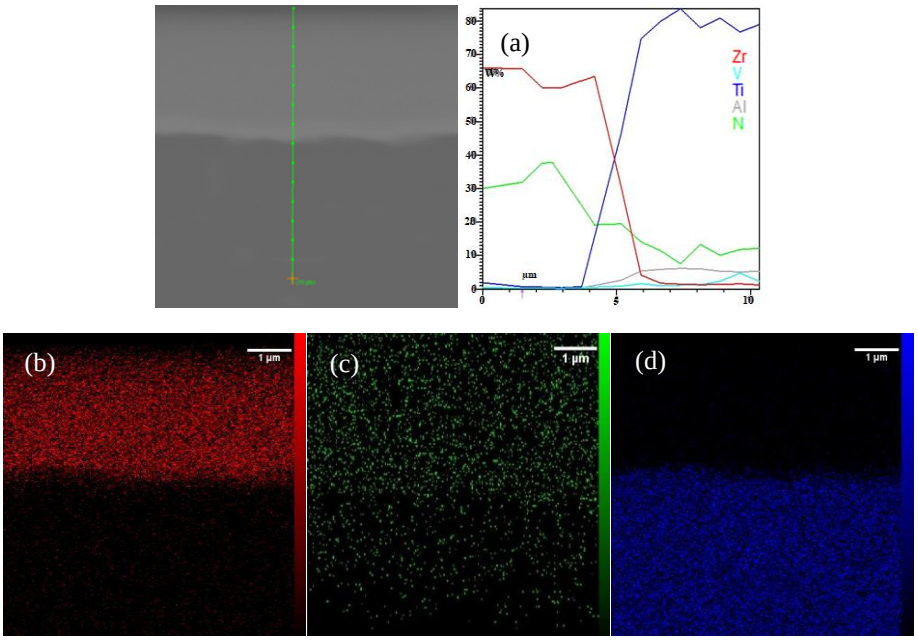

Figure 5 Cross-sectional EDS (a) line scan; (b) Zr; (c) N and (d) Ti, map analysis of ZrN single layer coating.

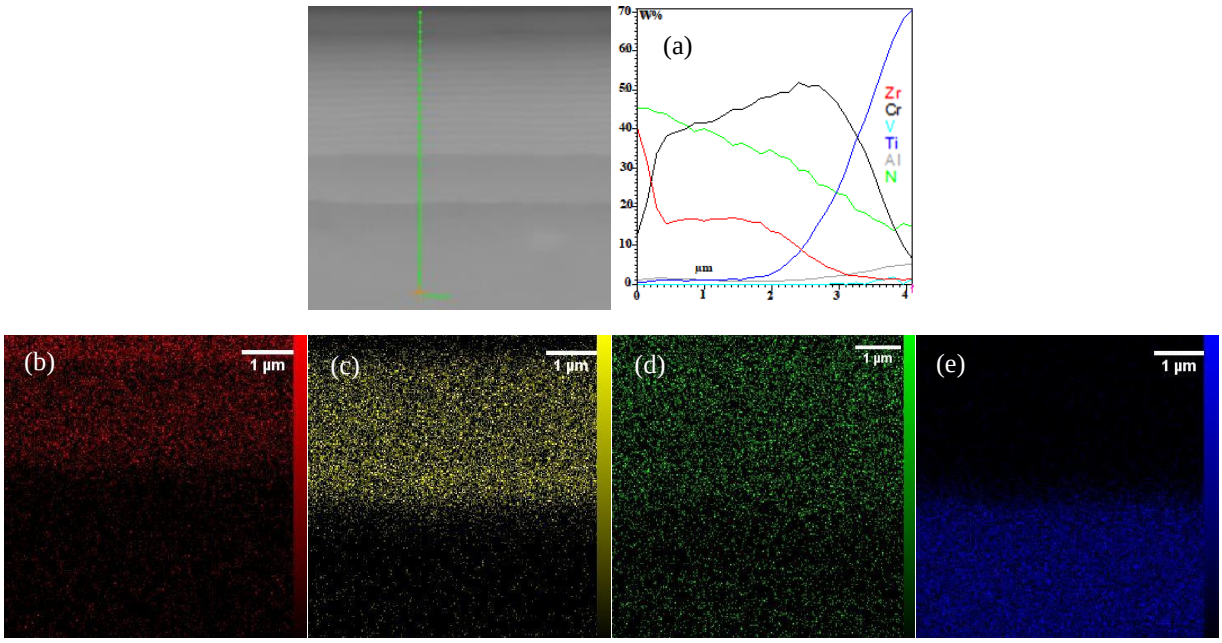

Figure 6 Cross-sectional EDS (a) line scan; (b) Zr; (c) Cr; (d) N and (e) Ti, map analysis of CrN/ZrN nanostructured multilayer coating.

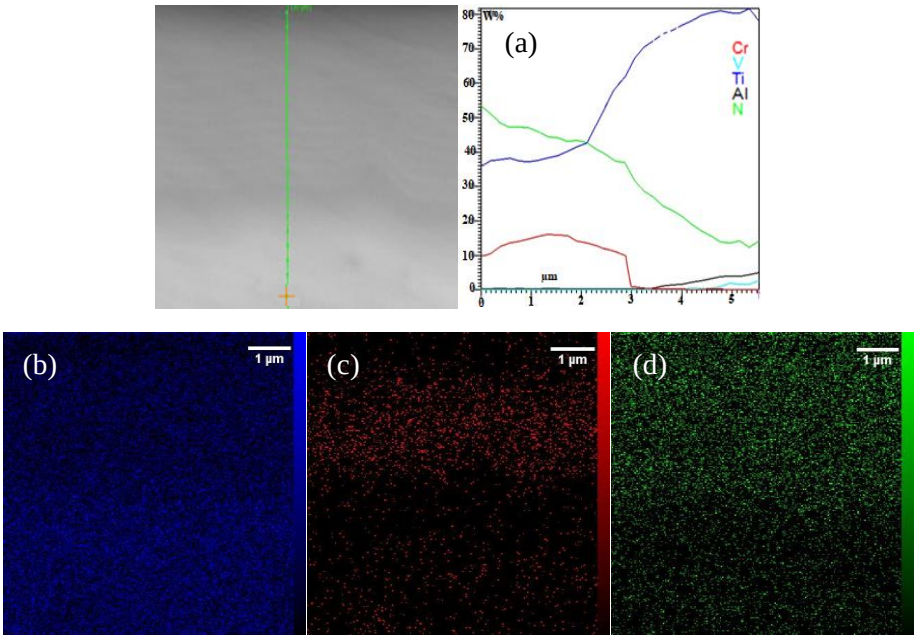

Figure 7 Cross-sectional EDS (a) line scan; (b) Ti; (c) Cr and (d) N, map analysis of CrN/TiN nanostructured multilayer coating.

3.3 Surface properties

3.3.1 Surface roughness

The surface roughness parameters and surface profile of all samples are given in Table 4 and Figure 8. As it is obvious from the FESEM observations, the coated samples with a TiN single layer and CrN/TiN nanostructured multilayer films exhibit rougher surfaces than the others.

Table 4. Surface roughness, microhardness, and contact angles values of the substrate and coated samples

Sample	Roughness(μm)		Microhardness(Gpa)	Contact angle(°)
	S_a	S_q		
Ti6Al4V	0.085±0.013	0.106±0.012	3.99±0.46	61.3±2 
TiN coated Ti6Al4V	0.214±0.031	0.267±0.031	23.08±0.84	74.4±3 
ZrN coated Ti6Al4V	0.072±0.014	0.096±0.011	20.74±0.76	65.4±3 
CrN/TiN coated Ti6Al4V	0.305±0.033	0.391±0.047	33.84±1.25	79.7±5 
CrN/ZrN coated Ti6Al4V	0.061±0.009	0.084±0.012	30.67±1.53	62.5±2 

The higher values of S_a and S_q for the coated samples with a TiN top layer are because of the presence of more microparticles and pinholes on them in comparison with the coated samples with a ZrN top layer [52]. As a consequence of the physical evaporation of vapor (PVD) method, it has been demonstrated in several studies that ZrN coating has a denser morphology than TiN [22,26] and CrN [50]. As a result, it is anticipated that coatings with a TiN top layer would be rougher than coatings with a ZrN top layer. The ZrN and CrN/ZrN coatings result in an average roughness of 60-70 nm that is close to that of “smooth” cemented orthopaedic implants[53] which are a case of relevant friction issues. The Sq/Sa ratio is close to 1.25 for the TiN and CrN/TiN coatings while it is higher for the ZrN and CrN/ZrN ones. This is evidence of a more rounded shape, close to a Gaussian height distribution, of the surface features of the former while they are sharper in the later cases.

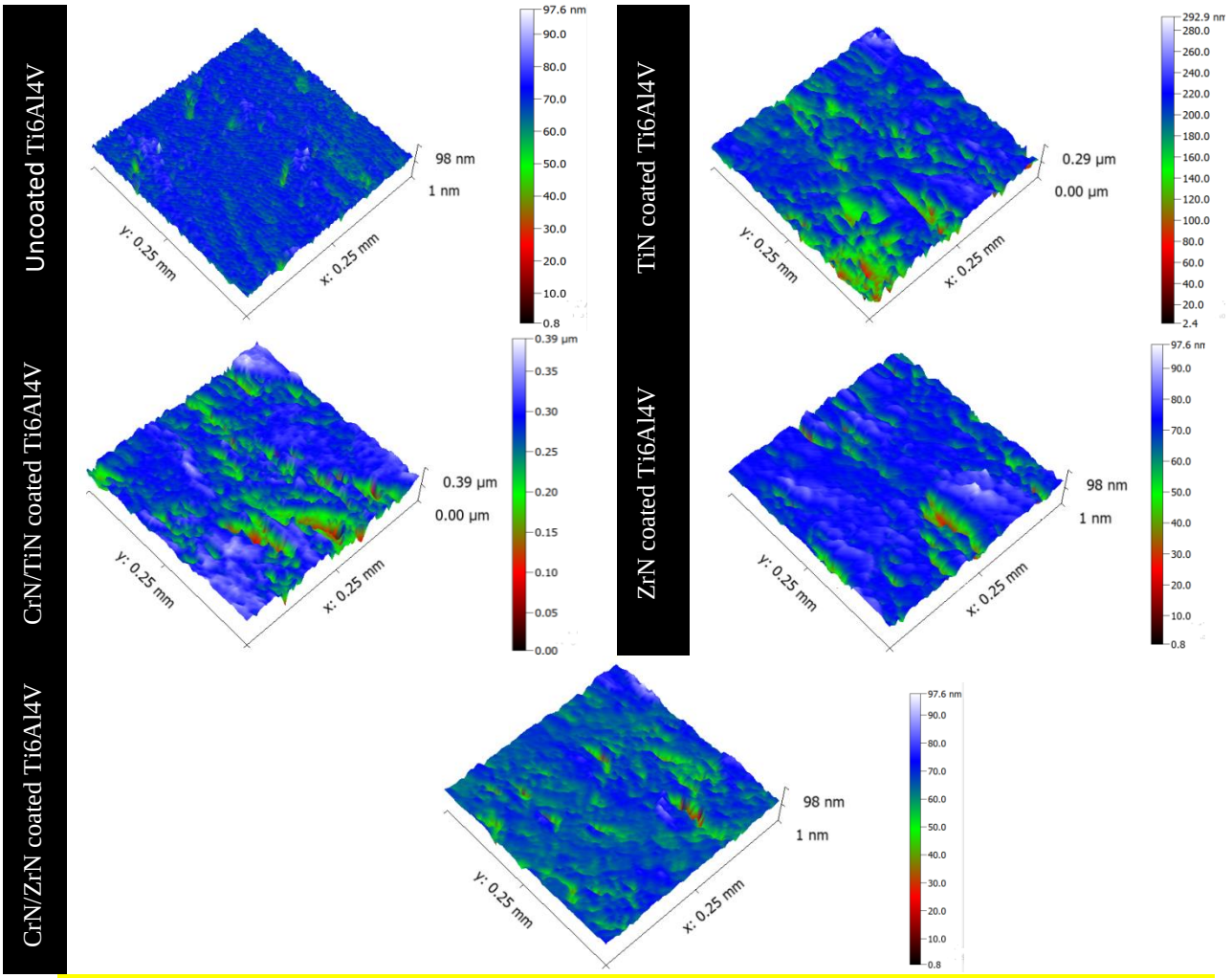

Figure 8 surface profile of uncoated and coated Ti6Al4V with TiN and ZrN single layers and CrN/TiN and CrN/ZrN nanostructured multilayer coatings.

3.3.2 Surface wettability

The results of wettability analysis, containing the water contact angles and water drops are presented in Table 4. All the tested surfaces can be classified as hydrophilic because the contact angles are all below the threshold of 90°. The measured contact angles of the coatings with a TiN top layer are slightly higher than those of the raw substrate and coatings with ZrN as a top layer. The little variations in contact angles observed can be mainly attributed to the differences in surface topography and roughness. Generally, the hydrophobicity or hydrophilicity of a surface is affected by surface chemical composition (contaminants from the atmosphere during deposition of the coating), roughness, and surface energy [54,55]. A micro- and nano-metric topography of a surface, which causes air trapping, can increase the contact angle whether the chemistry of the surface is more hydrophobic or lesser hydrophilic [56–58]. In this study, there are lots of microparticles and pinholes on the surface of the TiN single layer and CrN/TiN nanostructured multilayer coatings in comparison with the two others. Probably, more air will be trapped on the surface of them, and so this air trapping increases the hydrophobicity of the surface.

3.4 Hardness

The Knoop microhardness values for the substrate and all coated samples are presented in Table 4. Compared to the single layer coatings, higher hardness values were observed on the multilayer coatings similarly to those described elsewhere [33]. Additionally, the reported hardness values of the single layer coatings were significantly greater than those of the raw substrate because of the formation of a single-phase of TiN and ZrN as a hard layer on it.

The results are in accordance with the ones reported by Maksakova et al. [17] in their study based on the enhancement of the hardness value of the CrN/ZrN nanostructured multilayer coatings, in comparison with the CrN and ZrN single layers.

A large number of sharp and narrow interfaces act as barrier to movement of dislocations in these structures. Hence, an enhanced stress is needed for the dislocation movement [59]. Characterization of sputtered zirconium nitride films deposited at various argon: nitrogen ratio shows that the interfacial crystalline coherency and orientation of the individual monolayers also have a significant effect on the hardness value of these coatings [33]. When the shear modules of two layers, in a multilayer structure, are different, dislocations are positioned in the layer with a lower shear module because of the different dislocation line energy in them. In this circumstance, a stronger stress is required to move the dislocations to the layer with a higher shear module. Therefore, it would be difficult for dislocations to move across the interface of the two layers, increasing resistance to plastic deformation and, consequently, the hardness value of the coating [54].

Another factor, contributing to the high hardness of both the CrN/TiN and CrN/ZrN multilayer coatings, could be due to the presence of the Cr_2N phase with a hexagonal structure close to the CrN phase, with a cubic structure, in the CrN layers [17]. It can be expected that the high hardness values of these coatings lead to an improvement of their wear resistance [54].

3.5 Coatings adhesion

The results of the scratch tests (morphology of the tracks, acoustic emissions (A.E.), friction coefficients, and normal load graphs) are shown in Figure 9. A sharp increase in the A.E. signal was used for a first identification of the critical load (L_c), then it was confirmed, or eventually repositioned, by the SEM observation of the scratch tracks in correspondence of this load. On these samples, the L_c is not exactly on the point where the A.E. signal varies. This is because of some small cracks and fractures that occur on both sides of the scratch track before the coating being delaminated [16]. Referring to the sharp variation in A.E. signals and optical images, the measured values of L_c for CrN/TiN and CrN/ZrN nanostructured multilayer coatings are higher than those for single layers.

The SEM images collected from the surfaces of all the coatings clearly show the presence of radial cracks on the edges of the scratch tracks. Both a high compressive stress, in front of the indenter, and tensile stress, behind of it, cause these cracks to develop [60]. This behavior is because of the high hardness of the tested coatings [61]. The cracks appearing on the edge of the scratch track, parallel to the scratch direction, are tensile cracks that are much more present on

the single-layer TiN coating than in the ZrN one. Also, a recovery spallation failure can be observed in the scratch track of the ZrN coating. The recovery spallation failure gets stronger when the difference in the elasticity modules of the coating and the substrate is higher. Here, this condition is observable in the case of the ZrN single-layer coating. Additionally, conformal cracking can be clearly observed on the SEM images of the CrN/TiN and CrN/ZrN nanostructured multilayer coatings [61].

High residual compressive stress in CAE-PVD coatings could be a potent driving force toward coating separation when it is under load. So, decreasing the residual compressive stress within them is one of the effective approaches for increasing the adhesion strength of a coating to the substrate [15]. Deposition of alternating nanolayers, using interlayers, as well as adjusting them in number and thickness, might be effective in decreasing the compressive stress in addition to applying a bias voltage during the deposition process. For the single layer coatings, compression stresses are distributed in the whole thickness of the coating with the maximum value near the interface of the coating and substrate. While, the distribution is different in the structures consisting of nanolayers such as CrN/TiN and CrN/ZrN. The presence of these nanolayers prevents from stress accumulation and forms a gradient distribution of the stress. In these structures, the coating lifetime expands by controlling the crack growth through the "nanostructuration" of the stress field all along the thickness of the coating [19]. The presence of various interfaces in the nanostructured multilayer coatings and their function in preventing the mobility and propagation of cracks postpone the coating's destruction. Also, they may change the direction of the crack propagation in the film and limit it [60]. Finally, the higher hardness compared to single layers is also an effective parameter in their greater resistance to plastic deformation [60].

In present study, using of CrN, as a supportive layer in multilayer coatings, suggested that the upper layers have more loadbearing capacity and higher adhesion strength than single layer coatings. In the multilayer coatings, the presence of interlayers causes the failure mode to shift from brittle to ductile at the interface between the coating and substrate. Additionally, the use of –100 V bias voltage has a positive effect on the adhesion and cohesion of these coatings [62].

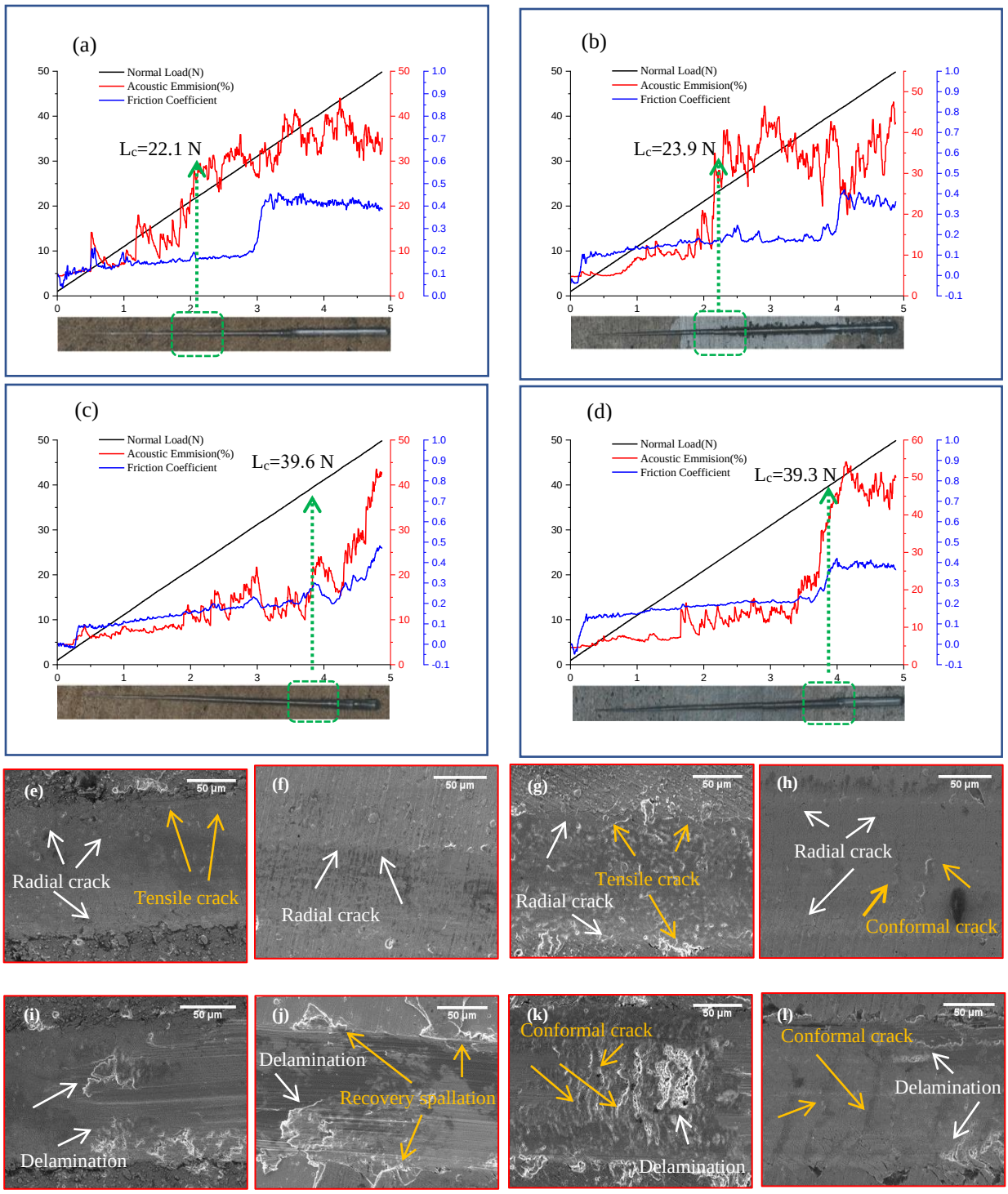

Figure 9Acoustic emission spectra and SEM images of scratch tracks for (a, e, i) TiN; (b, f, j) ZrN single layers; (c ,g, k) CrN/TiN and (d, h, l) CrN/ZrN nanostructured multilayer coatings.

3.6 In vitro bioactivity assessment

Bioactivity is an important factor influencing the bone bonding at the implant surface [63]. In this work, the bone-like apatite formation ability of different coatings has been examined after 14 days immersion in SBF. It needs to noate that the uncoated titanium and its alloys exhibited poor bioactivity [63].

Figure 10 displays the characteristic surface morphologies and EDS analysis of the surface of different tested samples. It can be seen that the uncoated Ti6Al4V alloy surface showed no visible or very few participates after soaking in SBF. Also, the Ca/P molar ratio is 1.16 which is much lower than the Ca/P ratio in stoichiometric hydroxyapatite. This indicates that mono calcium phosphate ($Ca(H_2PO_4)2H_2O$) or dicalcium phosphate ($Ca(HPO_4)H_2O$) were formed on the surface, based on previous investigations [64,65]. In contrast, the surfaces of all the coated samples were covered with apatite particles (floccule-like). According to EDS results, the presence of Ca and P was confirmed on the surface of all coatings. Ca/P ratio was 1.72±0.04 and 1.91±0.02 for TiN and ZrN single layers, respectively. This ratio was 1.89±0.07 and 1.8±0.04 for CrN/TiN and CrN/ZrN multilayer coatings, respectively. By comparison of the SEM images, it can be deduced that the number of apatite particles on the surface of the ZrN single layer and CrN/ZrN multilayers are more than those observed on the surface of TiN single layer and CrN/TiN multilayer coatings. This trend can be related to the special topography of the TiN single layer and CrN/TiN multilayer coatings (as described in section 3.2).

FTIR examinations were also conducted on different candidates after bioactivity tests. Adsorption bands corresponding to uncoated and coated surface groups are shown in Figure 11. FTIR adsorption spectrum of coated samples shows characteristic bands for hydroxyapatite. The presence of vibration bands at 562 and 600cm^{-1} are related to the symmetric bending vibration of $PO_4^{3-}(\upsilon_4)$, while the band at 867 cm^{-1} is a characteristic band for the symmetric stretching vibration of $PO4^{3-}(\ \upsilon_1)$ [66]. Also, the phosphate group at a range from 900 to 1200 cm^{-1} represents υ_3 stretching vibration for P-O [65]. The bands in a range from 1410 to 1470 and a weak peak at 1545 cm^{-1} are attributed to the υ_3 vibrations of CO_3^{2-} groups as a consequence of the substitution of CO_3^{2-} group with PO_4^{3-} group for B-type carbonated apatite [66]. The symmetric stretching vibration band of the HPO_4^{2-} group is observed at 1240 cm^{-1}[67]. The carbonyl group C=O is identified from the bands at 1712 cm^{-1}. The weak peak detected at 2850 can be assigned to ammonium ions [66]. The broadband for stretching mode (υ_5) of OH^- can be assigned at 3570-3853 cm^{-1}[67].

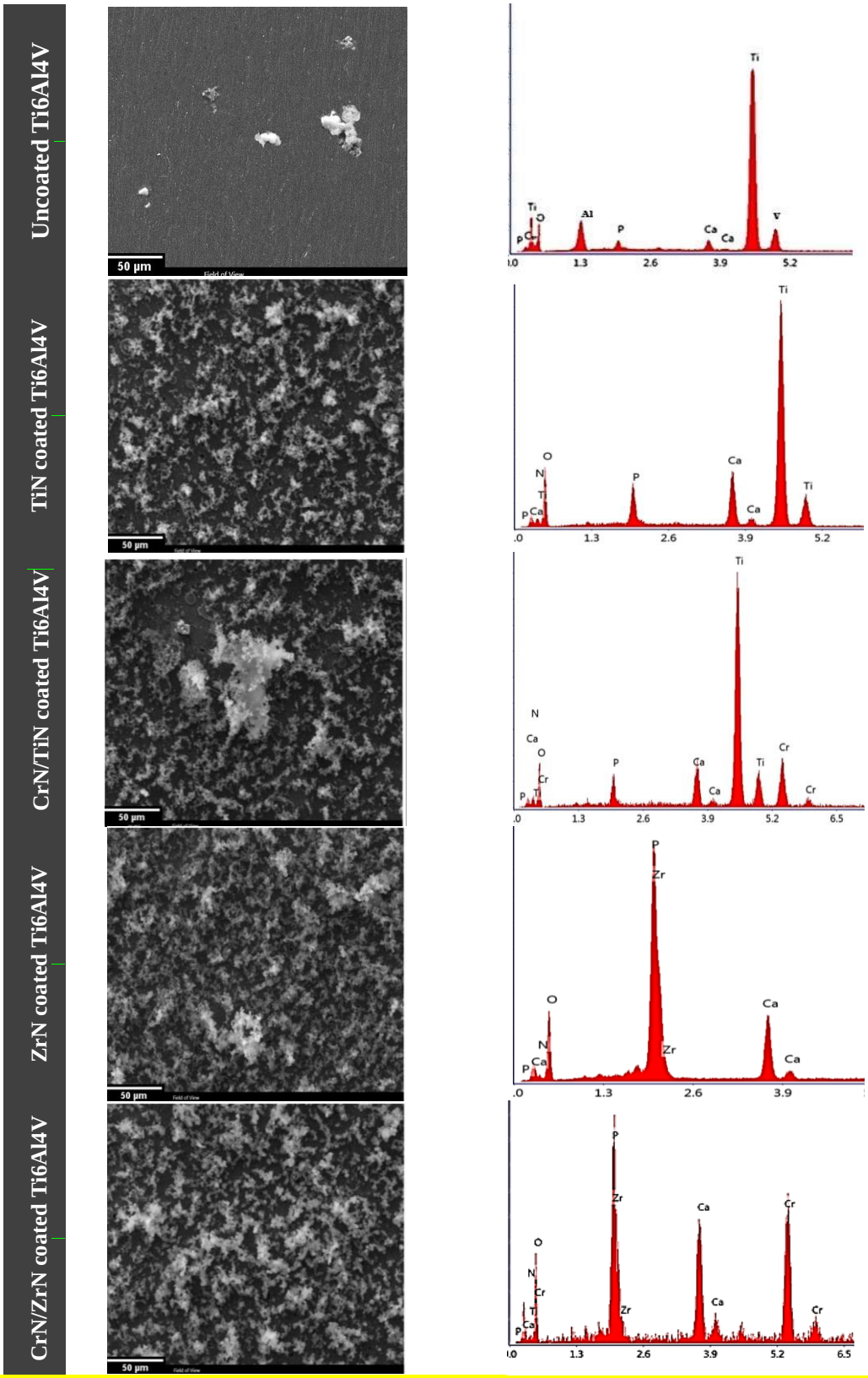

Figure 10 SEM surface micrographs and EDS analysis of uncoated and coated Ti–6Al–4V alloys after soaking in SBF for 14 days.

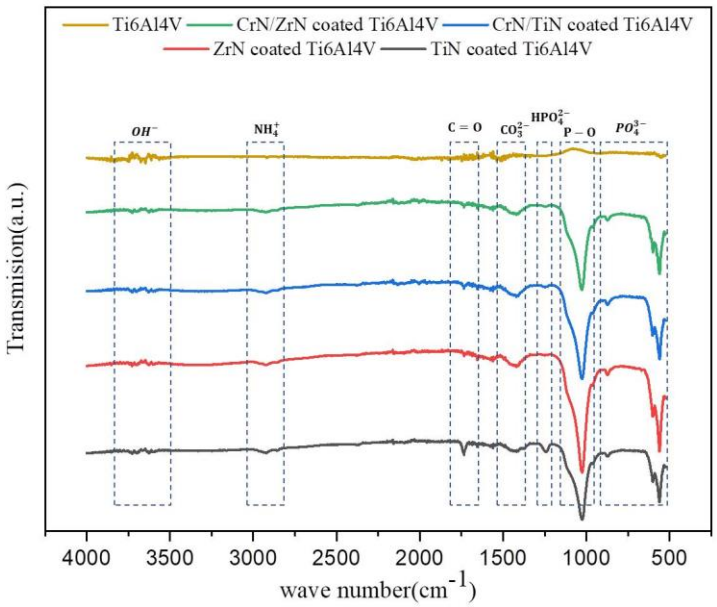

Figure 11 spectrum of the biomimetic apatite layer on the surface of the uncoated and coated Ti–6Al–4V alloys after 14 days immersion in SBF.

3.7 Electrochemical behaviour

PDP curves for uncoated and coated samples in SBF solution are shown in Figure 12. Extracted data from these curves, including the corrosion potential (E_{corr}), calculated by using the Tafel extrapolation method, corrosion current density(i_{corr}), polarization resistance (R_P), and protection efficiency (P_i%), are presented in Table5. Polarization resistance is an index of resistance to corrosion and it was calculated from the Stern-Geary formula for all the samples [68]. As it is clear from PDP curves, the corrosion potential and corrosion current density of the raw substrate have a shift to respectively more positive and lower values by applying the nitride coating on it. This suggests that nitride coatings reduce both the substrate corrosion driving force (thermodynamic effect) and corrosion rate (kinematic effect).

By the comparison of the curves of coated samples, it can be seen that their corrosion potentials are close to each other which means that their corrosion tendency in the mentioned environment is similar [69]. However, the values show the noblest behavior of the CrN/ZrN nanostructured multilayer coating in the SBF solution. The polarization resistance of this sample is also higher than the others and its corrosion current density is the lowest one. The values are 2.92×10^5 Ωcm^2 and 1.21×10^{-7} A/cm^2 , respectively. Meanwhile, the polarization resistance value and corrosion current density of the ZrN single layer and CrN/TiN nanostructured multilayer coatings are higher than the TiN single layer. This behavior may be understood as a result of the coatings' structure, morphology, and surface characteristics as described in section 3.2. Microparticles and pinholes, which are present in the coatings, are the most important weak

points of these surfaces when the coatings are in contact with corrosive solutions. They are considered to be the primary and main way for the corrosive electrolyte to pass through the substrate [9]. So the galvanic corrosion happens locally as a result of the formation of a galvanic cell between the anodic substrate and cathodic coating. Finally, the coating begins to separate from the substrate and, additionally, dissolution of the substrate ions happens [70]. According to what is above mentioned, the lower corrosion resistance and higher corrosion current density of the TiN single layer coating, compared to other coatings, is clearly understandable. As described in the previous sections, the surface FESEM images of the coatings with a TiN top part, showed numerous microparticles and pinholes on them. The ZrN single layer coating has shown higher corrosion resistance in the SBF solution, as expected. In general, the corrosion behavior of the coating is directly related to the surface defects, density, microstructure, and uniformity of the coating [71,72]. Accordingly, the smoother and more uniform surface of the ZrN single layer coating, with a lower density of defects in comparison to the TiN single layer coating, are the factors that made this coating more resistant to electrolyte penetration and corrosion [73].

The higher corrosion resistance of the CrN/TiN nanostructured multilayer coating compared to the TiN single layer, confirms that, in addition to the coating surface quality and surface defects density (number and size of microparticles and pinholes), some other factors affect the corrosion behavior of coatings. The peculiar architecture of nanostructured multilayer coatings provides a condition that, while the sample is exposed to the corrosive electrolyte, the penetration phenomenon takes a long time to reach the substrate (more than the single layers). Actually, the numerous interfaces which are in these coatings act as a barrier against the electrolyte and they improve the function of these coatings in the corrosive media [55]. The deposition of alternative layers from different materials prevents the formation of crystallites with continuous boundaries so that the possibility of the formation of cavities in the coating is reduced. The reduction of structural defects and blockage of defects of each layer by the next one are some effective factors that increase the corrosion resistance of nanostructured multilayer coatings in comparison with single layer structures. Therefore, it makes sense, given these explanations, that the CrN/TiN nanostructured multilayer coating has better polarization resistance than the TiN single layer and the CrN/ZrN nanostructured multilayer coating has higher polarization resistance than the ZrN single layer.

Despite the morphology of most PVD coatings is columnar, the CrN nanolayers have a non-columnar structure. So that the penetration of oxygen into these layers is limited and the corrosion process is postponed [72]. The presence of CrN nanolayers in the CrN/TiN and CrN/ZrN nanostructured multilayer coatings is hence another reason for their higher corrosion resistance of them compared to single layers.

According to all above explanations, the highest protection efficiency of CrN/ZrN nanostructured multilayer coating, which is calculated from the below relation, is justified [54].

$$P_i\% = \left[1 - \frac{i_{corr}}{i^0_{corr}}\right] \times 100$$

The i_{corr}, i^0_{corr} are the corrosion current density of the coated sample and substrate, respectively.

To complete the investigations, the amount of coating defects, which are known as porosity in the coatings, was calculated from the formula [55]:

$$p\% = \frac{R_{ps}}{R_{pc}} \times 10^{-(\frac{\Delta E_{corr}}{\beta_a})}$$

In the above relation, p% demonstrates the coating porosity, R_{ps} and R_{pc} are the polarization resistances of the raw substrate and coated sample, respectively. ΔE_{corr} Shows the corrosion potential variations and β_a is the anodic region slope in the raw substrate curve. As it is known from

Figure 13, the CrN/ZrN nanostructured multilayer coating has the least pore density (0.009%), ZrN is after it in the list, with a value of 0.024%, then the CrN/TiN nanostructured multilayer coating has a value of 0.038%, and the maximum porosity percentage is for the TiN single layer (0.107%). These findings indicate that the CrN/ZrN nanostructured multilayer coating has the maximum corrosion resistance due to its structure's negligible porosity.

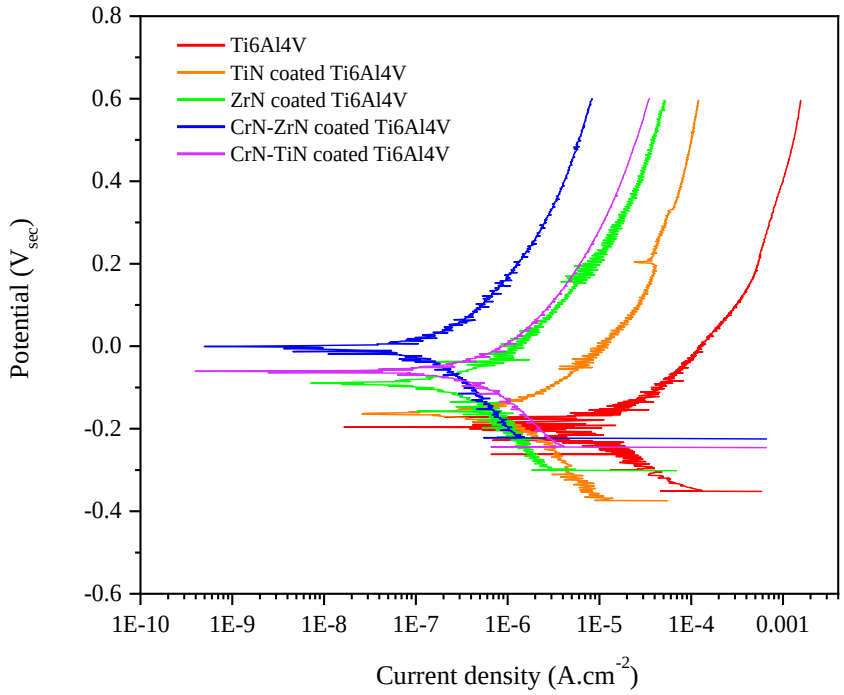

Figure 12 PDP plots of the coated and uncoated Ti6Al4V in SBF solution.

Table5. Electrochemical parameters extracted from the PDP plots

sample	E_{corr} (V)	i_{corr} (Acm^{-2})	R_p ($\Omega.cm^2$)	P_i (%)
Ti6Al4V	-0.19	1.35×10^{-5}	2.83×10^{3}	-
TiN coated Ti6Al4V	-0.17	1.73×10^{-6}	2.54×10^{4}	87.18
ZrN coated Ti6Al4V	-0.01	4.57×10^{-7}	1.13×10^{5}	96.67
CrN/TiN coated Ti6Al4V	-0.07	4.76×10^{-7}	1.13×10^{5}	96.47
CrN/ZrN coated Ti6Al4V	-0.03	1.21×10^{-7}	2.92×10^{5}	99.11

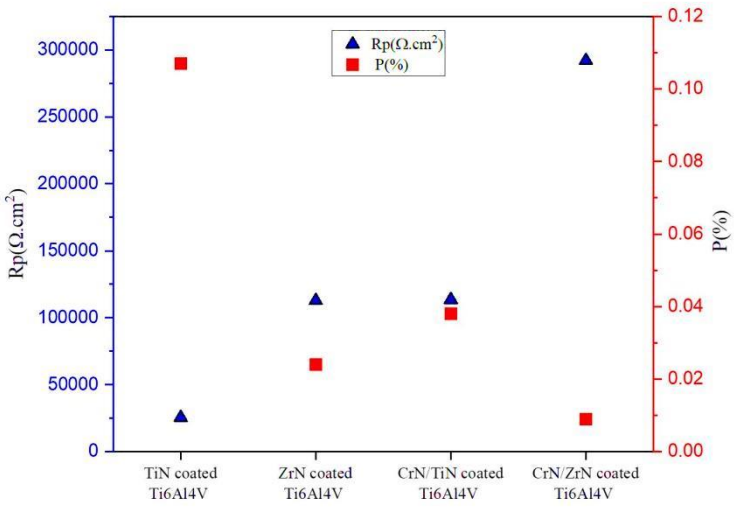

Figure 13 R_p and p% of coated samples.

Figure 14 shows the Nyquist, Bode-impendence, and Bode-phase plots of the uncoated and coated Ti6Al4V after immersion in the SBF solution for 30 minutes in open circuit potential. All the tested samples exhibited typical capacitive behavior. The diameter of the Nyquist plot can be used as an interpretation of the corrosion resistance [74].

Among all the tested samples, CrN/ZrN coating exhibited the best corrosion performance based on the appearance of largest semicircle diameter in Nyquist plots. As shown in Figure 14, TiN single layer exhibited the smallest diameter of impedance arc, when compared with other coatings. The presence of some defects such as pinholes and pores in the coating deteriorated the corrosion resistance of TiN and ZrN coatings. However, the presence of alternative layers in the case of CrN/ZrN and CrN/TiN multilayer coatings strongly improved the anti-corrosion properties.

Based on previous works[21], two- time constants equivalent electrical circuit (ESC) was used for fitting the EIS data (Figure 15). The extracted data are summarized in Table 6. The EEC includes R_s, solution resistance, CPE_1 and CPE_2, constant phase element of the coating (oxide layer for Ti6Al4V), and electrical double layer, respectively. It also includes R_1 and R_2 which are the resistance of pore in the coatings (oxide layer for Ti6Al4V) and charge transfer resistance,

respectively. According to Table 6, the nanostructured multilayer CrN/ZrN coating demonstrated a superior polarization resistance compared to other coatings.

According to the Bode-phase plots in Figure 14, the maximum phase angle at high frequency range has been increased for multilayer coatings, meaning that these coatings were more compact.

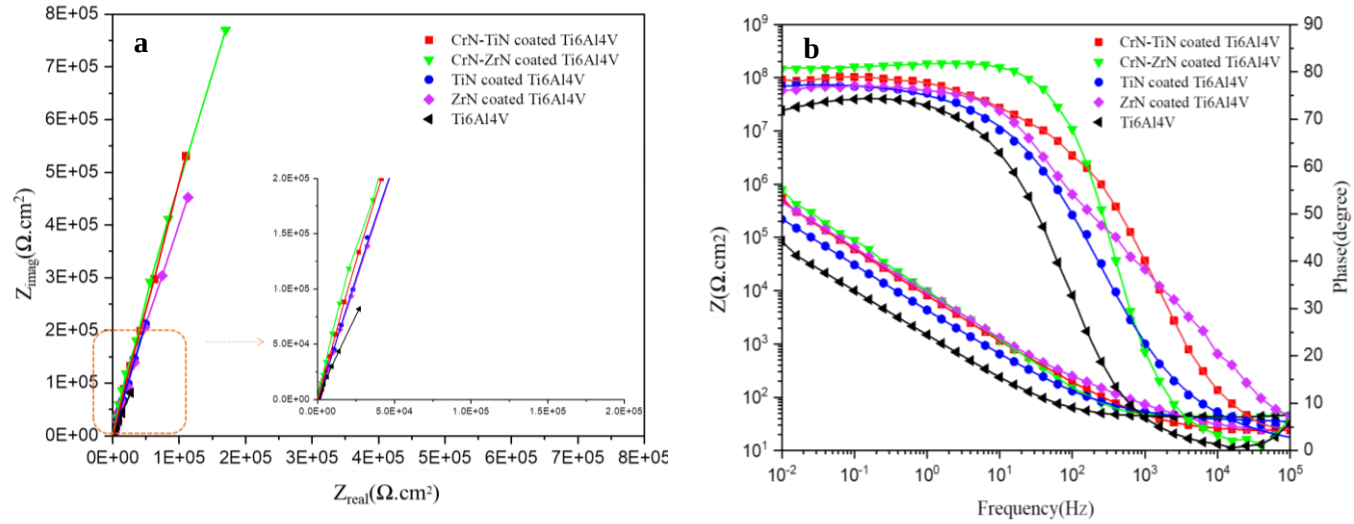

Figure 14 (a) Nyquist and (b) bode plots of the uncoated and coated samples in SBF solution.

Table 6. Extracted EIS parameters of the uncoated and coated samples from the considered EEC

Coating	R_s ($\Omega.cm^2$)	CPE_1 ($s^n.\Omega^{-1}.cm^{-2}$)	R_1 ($\Omega.cm^2$)	CPE_2 ($s^n.\Omega^{-1}.cm^{-2}$)	R_2 ($\Omega.cm^2$)	R_p ($\Omega.cm^2$)	χ^2
Ti6Al4V	42.7	1.6×10^{-3}	2.6×10^{3}	1.5×10^{-4}	6.3×10^{5}	6.3×10^{5}	8.9×10^{-3}
TiN coated Ti6Al4V	39.8	5.4×10^{-4}	1.0×10^{4}	5.2×10^{-5}	1.7×10^{6}	1.7×10^{6}	1.6×10^{-3}
ZrN coated Ti6Al4V	40.7	1.4×10^{-4}	6.8×10^{4}	2.7×10^{-5}	5.0×10^{6}	5.1×10^{6}	6.2×10^{-3}
CrN/TiN coated Ti6Al4V	38.7	3.7×10^{-4}	5.5×10^{4}	2.6×10^{-5}	5.7×10^{6}	5.8×10^{6}	2.4×10^{-3}
CrN/ZrN coated Ti6Al4V	42.1	9.83×10^{-5}	9.7×10^{5}	2.2×10^{-5}	1.3×10^{7}	1.3×10^{7}	6.5×10^{-3}

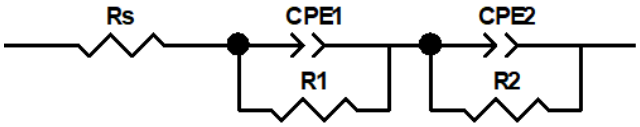

Figure 15 Best equivalent electrical circuit used for simulating the experimental impedance data.

4. Conclusions

In the present study, TiN and ZrN single layer and CrN/TiN and CrN/ZrN nanostructured multilayer coatings were deposited on a Ti6Al4V alloy substrate by CAE-PVD method. According to the findings, the coated samples with a TiN top layer exhibited higher roughness than two other coatings why so more amount of microparticles were found on them. Also the

higher contact angles were recorded for them. It was suggested that this behavior is related to more air trapping on their surface. The results of microhardness test showed the higher hardness for two multilayer coatings in comparison with single layers. The scratch tests revealed that the critical load values obtained for CrN/TiN and CrN/ZrN nanostructured multilayer coatings were higher than those observed for the single layers. Based on the bioactivity evaluations, ZrN single layer and CrN/ZrN multilayer coatings showed a better hydroxyapatite precipitation; however, all surfaces had satisfactory bioactivity. Corrosion examinations revealed that CrN/ZrN multilayer coating exhibited the best corrosion resistance among all the tested samples due to its smoother surface and more dense structure in addition to its specific architecture. Hence, CrN/ZrN multilayer coatings investigated in this study has promising bioactivity and corrosion resistance properties and is potentially good candidate for biomedical applications.

Acknowledgments

This research was conducted partly at materials engineering faculty of Isfahan University of Technology and partly at Department of Applied Science and Technology of Polytechnic University of Turin. Authors would like to thank the technicians of relevant laboratories. Presence in Polytechnic University of Turin and conducting the research was done in the form of ERASMUS^{+} mobility program (funded by European Education and Culture Executive Agency).

References

[1] R. Bahi, C. Nouveau, N.E. Beliardouh, C.E. Ramoul, S. Meddah, O. Ghelloudj, Surface performances of Ti-6Al-4V substrates coated PVD multilayered films in biological environments, Surf. Coatings Technol. 385 (2020) 125412. https://doi.org/10.1016/j.surfcoat.2020.125412.

[2] L. Floroian, D. Craciun, G. Socol, G. Dorcioman, M. Socol, M. Badea, V. Craciun, Titanium implants' surface functionalization by pulsed laser deposition of TiN, ZrC and ZrN hard films, Appl. Surf. Sci. 417 (2017) 175–182. https://doi.org/10.1016/j.apsusc.2017.03.068.

[3] M.Z. Ibrahim, A.A.D. Sarhan, F. Yusuf, M. Hamdi, Biomedical materials and techniques to improve the tribological, mechanical and biomedical properties of orthopedic implants – A review article, J. Alloys Compd. 714 (2017) 636–667. https://doi.org/10.1016/j.jallcom.2017.04.231.

[4] M.F. Kunrath, T.C. Muradás, N. Penha, M.M. Campos, Innovative surfaces and alloys for dental implants: What about biointerface-safety concerns?, Dent. Mater. 37 (2021) 1447–1462. https://doi.org/10.1016/j.dental.2021.08.008.

[5] N. Lin, X. Huang, X. Zhang, A. Fan, L. Qin, B. Tang, In vitro assessments on bacterial adhesion and corrosion performance of TiN coating on Ti6Al4V titanium alloy synthesized by multi-arc ion plating, Appl. Surf. Sci. 258 (2012) 7047–7051. https://doi.org/10.1016/j.apsusc.2012.03.163.

[6] R. Olivares-Navarrete, J.J. Olaya, C. Ramírez, S.E. Rodil, Biocompatibility of niobium coatings, Coatings. 1 (2011) 72–87. https://doi.org/10.3390/coatings1010072.

[7] S. Datta, M. Das, V.K. Balla, S. Bodhak, V.K. Murugesan, Mechanical, wear, corrosion and biological properties of arc deposited titanium nitride coatings, Surf. Coatings Technol. 344 (2018) 214–222. https://doi.org/10.1016/j.surfcoat.2018.03.019.

[8] M. Fellah, L. Aissani, M.A. Samad, S. Mechacheti, M.Z. Touhami, A. Montagne, A. Iost, Characterisation of R.F. magnetron sputtered Cr-N, Cr-Zr-N and Zr-N coatings, Trans. Inst. Met. Finish. 95 (2017) 261–268. https://doi.org/10.1080/00794236.2017.1339464.

[9] A. Gilewicz, P. Chmielewska, D. Murzynski, E. Dobruchowska, B. Warcholinski, Corrosion resistance of CrN and CrCN/CrN coatings deposited using cathodic arc evaporation in Ringer's and Hank's solutions, Surf. Coatings Technol. 299 (2016) 7–14. https://doi.org/10.1016/j.surfcoat.2016.04.069.

[10] P.E. Hovsepian, A.P. Ehiasarian, Y. Purandare, A.A. Sugumaran, T. Marriott, I. Khan, Development of superlattice CrN/NbN coatings for joint replacements deposited by high power impulse magnetron sputtering, J. Mater. Sci. Mater. Med. 27 (2016). https://doi.org/10.1007/s10856-016-5751-0.

[11] P.E. Hovsepian, A.A. Sugumaran, M. Rainforth, J. Qi, I. Khan, A.P. Ehiasarian, Microstructure and load bearing capacity of TiN/NbN superlattice coatings deposited on medical grade CoCrMo alloy by HIPIMS, J. Mech. Behav. Biomed. Mater. 132 (2022) 105267. https://doi.org/10.1016/j.jmbbm.2022.105267.

[12] R.P. Van Hove, I.N. Sierevelt, B.J. Van Royen, P.A. Nolte, Titanium-Nitride Coating of Orthopaedic Implants: A Review of the Literature, Biomed Res. Int. 2015 (2015). https://doi.org/10.1155/2015/485975.

[13] F. Hollstein, P. Louda, Bio-compatible low reflective coatings for surgical tools using reactive d.c.-magnetron sputtering and arc evaporation - a comparison regarding steam sterilization resistance and nickel diffusion, Surf. Coatings Technol. 120–121 (1999) 672–681. https://doi.org/10.1016/S0257-8972(99)00357-6.

[14] H. Olia, R. Ebrahimi-Kahrizsangi, F. Ashrafizadeh, I. Ebrahimzadeh, Corrosion study of TiN, TiAlN and CrN multilayer coatings deposit on martensitic stainless steel by arc cathodic physical vapour deposition, Mater. Res. Express. 6 (2019) 046425. https://doi.org/10.1088/2053-1591/aaff11.

[15] C. Mendibide, P. Steyer, J. Fontaine, P. Goudeau, Improvement of the tribological behaviour of PVD nanostratified TiN/CrN coatings - An explanation, Surf. Coatings Technol. 201 (2006) 4119–4124. https://doi.org/10.1016/j.surfcoat.2006.08.013.

[16] P.L. Sun, C.Y. Su, T.P. Liou, C.H. Hsu, C.K. Lin, Mechanical behavior of TiN/CrN nano-multilayer thin film deposited by unbalanced magnetron sputter process, J. Alloys Compd.

509 (2011) 3197–3201. https://doi.org/10.1016/j.jallcom.2010.12.057.

[17] O. V. Maksakova, S. Simoẽs, A.D. Pogrebnjak, O. V. Bondar, Y.O. Kravchenko, T.N. Koltunowicz, Z.K. Shaimardanov, Multilayered ZrN/CrN coatings with enhanced thermal and mechanical properties, J. Alloys Compd. 776 (2019) 679–690. https://doi.org/10.1016/j.jallcom.2018.10.342.

[18] C. Liu, A. Leyland, Q. Bi, A. Matthews, Corrosion resistance of multi-layered plasma-assisted physical vapour deposition TiN and CrN coatings, Surf. Coatings Technol. 141 (2001) 164–173. https://doi.org/10.1016/S0257-8972(01)01267-1.

[19] C. Zhao, Y. Zhu, Z. Yuan, J. Li, Structure and tribocorrosion behavior of Ti/TiN multilayer coatings in simulated body fluid by arc ion plating, Surf. Coatings Technol. 403 (2020) 126399. https://doi.org/10.1016/j.surfcoat.2020.126399.

[20] B.O. Postolnyi, V.M. Beresnev, G. Abadias, O. V. Bondar, L. Rebouta, J.P. Araujo, A.D. Pogrebnjak, Multilayer design of CrN/MoN protective coatings for enhanced hardness and toughness, J. Alloys Compd. 725 (2017) 1188–1198. https://doi.org/10.1016/j.jallcom.2017.07.010.

[21] P.M. Samim, A. Fattah-alhosseini, H. Elmkhah, O. Imantalab, M. Nouri, A study on comparing surface characterization and electrochemical properties of single-layer CrN coating with nanostructured multilayer ZrN/CrN coating in 3.5 wt.% NaCl solution, Surfaces and Interfaces. 21 (2020) 100721. https://doi.org/10.1016/j.surfin.2020.100721.

[22] O. Maksakova, S. Simoẽs, A. Pogrebnjak, O. Bondar, Y. Kravchenko, V. Beresnev, N. Erdybaeva, The influence of deposition conditions and bilayer thickness on physical-mechanical properties of CA-PVD multilayer ZrN/CrN coatings, Mater. Charact. 140 (2018) 189–196. https://doi.org/10.1016/j.matchar.2018.03.048.

[23] S. Kumar, S.R. Maity, L. Patnaik, Effect of tribological process parameters on the wear and frictional behaviour of Cr-(CrN/TiN) composite coating: An experimental and analytical study, Ceram. Int. 47 (2021) 16018–16028. https://doi.org/10.1016/j.ceramint.2021.02.176.

[24] Gholamreza Faghani, S.M. Rabiee, S. Nourouzi, H. Elmkhah, Nanoscale Multi-Layer Thin Film Fabricated by Cathodic Arc Evaporation (CAE) Method, J. Superhard Mater. 42 (2020) 78–89. https://doi.org/10.3103/S1063457620020057.

[25] J. An, Q.Y. Zhang, Structure, morphology and nanoindentation behavior of multilayered TiN/TaN coatings, Surf. Coatings Technol. 200 (2005) 2451–2458. https://doi.org/10.1016/j.surfcoat.2005.02.204.

[26] J. An, Q.Y. Zhang, Structure, hardness and tribological properties of nanolayered TiN/TaN multilayer coatings, Mater. Charact. 58 (2007) 439–446. https://doi.org/10.1016/j.matchar.2006.06.012.

[27] C.E. Tsai, J. Hung, Y. Hu, D.Y. Wang, R.M. Pilliar, R. Wang, Improving fretting corrosion resistance of CoCrMo alloy with TiSiN and ZrN coatings for orthopedic applications, J. Mech. Behav. Biomed. Mater. 114 (2021) 104233. https://doi.org/10.1016/j.jmbbm.2020.104233.

[28] N.S. Mansoor, A. Fattah-alhosseini, H. Elmkhah, A. Shishehian, Electrochemical behavior of TiN, CrN and TiN/CrN nanostructured coatings on the nickel-chromium alloy used in dental fixed prosthesis, J. Asian Ceram. Soc. 8 (2020) 694–710. https://doi.org/10.1080/21870764.2020.1776915.

[29] Z.A. Fazel, H. Elmkhah, A. Fattah-Alhosseini, K. Babaei, M. Meghdari, Comparing electrochemical behavior of applied CrN/TiN nanoscale multilayer and TiN single-layer coatings deposited by CAE-PVD method, J. Asian Ceram. Soc. 8 (2020) 510–518. https://doi.org/10.1080/21870764.2020.1756065.

[30] T. Rajabi, M. Atapour, H. Elmkhah, S. Mehran, Nanometric CrN / CrAlN and CrN / ZrN multilayer physical vapor deposited coatings on 316L stainless steel as bipolar plate for proton exchange membrane fuel cells, 753 (2022).

[31] S. Jannat, H. Rashtchi, M. Atapour, M.A. Golozar, H. Elmkhah, M. Zhiani, Preparation and performance of nanometric Ti/TiN multi-layer physical vapor deposited coating on 316L stainless steel as bipolar plate for proton exchange membrane fuel cells, J. Power Sources. 435 (2019) 226818. https://doi.org/10.1016/j.jpowsour.2019.226818.

[32] Y. Vengesa, A. Fattah-alhosseini, H. Elmkhah, O. Imantalab, M.K. Keshavarz, Investigation of corrosion and tribological characteristics of annealed CrN/CrAlN coatings deposited by CAE-PVD, Ceram. Int. 49 (2023) 3016–3029. https://doi.org/10.1016/j.ceramint.2022.09.286.

[33] D. Arias, A. Devia, J. Velez, Study of TiN/ZrN/TiN/ZrN multilayers coatings grown by cathodic arc technique, Surf. Coatings Technol. 204 (2010) 2999–3003. https://doi.org/10.1016/j.surfcoat.2010.03.033.

[34] P. Mohamadian Samim, A. Fattah-Alhosseini, H. Elmkhah, O. Imantalab, Structure and corrosion behavior of ZrN/CrN nano-multilayer coating deposited on AISI 304 stainless steel by CAE-PVD technique, J. Asian Ceram. Soc. 8 (2020) 460–469. https://doi.org/10.1080/21870764.2020.1750102.

[35] N.S. Mansoor, A. Fattah-Alhosseini, H. Elmkhah, A. Shishehian, Comparison of the mechanical properties and electrochemical behavior of TiN and CrN single-layer and CrN/TiN multi-layer coatings deposited by PVD method on a dental alloy, Mater. Res. Express. 6 (2019). https://doi.org/10.1088/2053-1591/ab640d.

[36] M. Soleimani, A. Fattah-alhosseini, H. Elmkhah, K. Babaei, O. Imantalab, A comparison of tribological and corrosion behavior of PVD-deposited CrN/CrAlN and CrCN/CrAlCN nanostructured coatings, Ceram. Int. 49 (2023) 5029–5041. https://doi.org/10.1016/j.ceramint.2022.10.016.

[37] P.M. Samim, A. Fattah-alhosseini, H. Elmkhah, O. Imantalab, Nanoscale architecture of ZrN/CrN coatings: microstructure, composition, mechanical properties and electrochemical behavior, J. Mater. Res. Technol. 15 (2021) 542–560. https://doi.org/10.1016/j.jmrt.2021.08.018.

[38] B. Subramanian, Enhancement of biocompatibility of metal implants by nanoscale TiN/NbN multilayer coatings, J. Nanosci. Nanotechnol. 13 (2013) 4565–4572. https://doi.org/10.1166/jnn.2013.7170.

[39] A. Vladescu, A. Kiss, M. Braic, C.M. Cotrut, P. Drob, M. Balaceanu, C. Vasilescu, V. Braic, Vacuum arc deposition of nanostructured multilayer coatings for biomedical applications, J. Nanosci. Nanotechnol. 8 (2008) 733–738. https://doi.org/10.1166/jnn.2008.D211.

[40] H. Ma, Q. Miao, G. Zhang, W. Liang, Y. Wang, Z. Sun, H. Lin, The influence of multilayer structure on mechanical behavior of TiN/TiAlSiN multilayer coating, Ceram. Int. 47 (2021) 12583–12591. https://doi.org/10.1016/j.ceramint.2021.01.117.

[41] J. Zheng, J. Hao, X. Liu, Q. Gong, W. Liu, A thick TiN/TiCN multilayer film by DC magnetron sputtering, Surf. Coatings Technol. 209 (2012) 110–116. https://doi.org/10.1016/j.surfcoat.2012.08.045.

[42] T. Kokubo, H. Takadama, How useful is SBF in predicting in vivo bone bioactivity?, Biomaterials. 27 (2006) 2907–2915. https://doi.org/10.1016/j.biomaterials.2006.01.017.

[43] M.P. Nikolova, V. Nikolova, V.L. Ivanova, S. Valkov, P. Petrov, M.D. Apostolova, Mechanical properties and in vitro biocompatibility evaluation of TiN/TiO2coated Ti6Al4V alloy, Mater. Today Proc. 33 (2020) 1781–1786. https://doi.org/10.1016/j.matpr.2020.05.051.

[44] S.H. Huang, S.F. Chen, Y.C. Kuo, C.J. Wang, J.W. Lee, Y.C. Chan, H.W. Chen, J.G. Duh, T.E. Hsieh, Mechanical and tribological properties evaluation of cathodic arc deposited CrN/ZrN multilayer coatings, Surf. Coatings Technol. 206 (2011) 1744–1752. https://doi.org/10.1016/j.surfcoat.2011.10.029.

[45] B. Warcholiński, A. Gilewicz, Z. Kukliński, P. Myśliński, Arc-evaporated CrN, CrN and CrCN coatings, Vacuum. 83 (2008) 715–718. https://doi.org/10.1016/j.vacuum.2008.05.005.

[46] A.K. Krella, Cavitation erosion of monolayer PVD coatings – An influence of deposition technique on the degradation process, Wear. 478–479 (2021) 203762. https://doi.org/10.1016/j.wear.2021.203762.

[47] R. Tian, J. Sun, Corrosion resistance and interfacial contact resistance of TiN coated 316L bipolar plates for proton exchange membrane fuel cell, Int. J. Hydrogen Energy. 36 (2011) 6788–6794. https://doi.org/10.1016/j.ijhydene.2011.03.021.

[48] X. Bai, L. Xu, X. Shi, J. Ren, L. Xu, Q. Wang, B. Li, Z. Liu, C. Zheng, Q. Fu, Hydrothermal oxidation improves corrosion and wear properties of multi-arc ion plated titanium nitride coating for biological application, Vacuum. 198 (2022) 110871. https://doi.org/10.1016/j.vacuum.2022.110871.

[49] W.D. Münz, I.J. Smith, D.B. Lewis, S. Creasey, Droplet formation on steel substrates during cathodic steered arc metal ion etching, Vacuum. 48 (1997) 473–481. https://doi.org/10.1016/s0042-207x(96)00307-7.

[50] Z.G. Zhang, O. Rapaud, N. Allain, D. Mercs, M. Baraket, C. Dong, C. Coddet, Microstructures and tribological properties of CrN/ZrN nanoscale multilayer coatings, Appl. Surf. Sci. 255 (2009) 4020–4026. https://doi.org/10.1016/j.apsusc.2008.10.075.

[51] C.K. Lin, C.H. Hsu, S.C. Kung, Effect of electroless nickel interlayer on wear behavior of

CrN/ZrN multilayer films on Cu-alloyed ductile iron, Appl. Surf. Sci. 284 (2013) 59–65. https://doi.org/10.1016/j.apsusc.2013.06.167.

[52] N.A. Baseri, M. Mohammadi, M. Ghatee, M. Abassi-Firouzjah, H. Elmkhah, The effect of duty cycle on the mechanical and electrochemical corrosion properties of multilayer CrN/CrAlN coatings produced by cathodic arc evaporation, Surf. Eng. 37 (2021) 253–262. https://doi.org/10.1080/02670844.2020.1775331.

[53] M. Hirata, K. Oe, A. Kaneuji, R. Uozu, K. Shintani, T. Saito, Relationship between the surface roughness of material and bone cement: An increased “polished” stem may result in the excessive taper-slip, Materials (Basel). 14 (2021). https://doi.org/10.3390/ma14133702.

[54] O. Çomaklı, Improved structural, mechanical, corrosion and tribocorrosion properties of Ti45Nb alloys by TiN, TiAlN monolayers, and TiAlN/TiN multilayer ceramic films, Ceram. Int. 47 (2021) 4149–4156. https://doi.org/10.1016/j.ceramint.2020.09.292.

[55] S.P. Mani, P. Agilan, M. Kalaiarasan, K. Ravichandran, N. Rajendran, Y. Meng, Effect of multilayer CrN/CrAlN coating on the corrosion and contact resistance behavior of 316L SS bipolar plate for high temperature proton exchange membrane fuel cell, J. Mater. Sci. Technol. 97 (2022) 134–146. https://doi.org/10.1016/j.jmst.2021.04.043.

[56] L. Jiang, Y. Zhao, J. Zhai, A Lotus-Leaf-like Superhydrophobic Surface: A Porous Microsphere/Nanofiber Composite Film Prepared by Electrohydrodynamics, Angew. Chemie. 116 (2004) 4438–4441. https://doi.org/10.1002/ange.200460333.

[57] B. Lu, N. Li, Versatile aluminum alloy surface with various wettability, Appl. Surf. Sci. 326 (2015) 168–173. https://doi.org/10.1016/j.apsusc.2014.11.138.

[58] N.P. Patel, K. V. Chauhan, J.M. Kapopara, N.N. Jariwala, S.K. Rawal, Characterization of sputtered zirconium nitride films deposited at various argon:nitrogen ratio, IOP Conf. Ser. Mater. Sci. Eng. 149 (2016). https://doi.org/10.1088/1757-899X/149/1/012015.

[59] Y.Y. Chang, D.Y. Wang, C.Y. Hung, Structural and mechanical properties of nanolayered TiAlN/CrN coatings synthesized by a cathodic arc deposition process, Surf. Coatings Technol. 200 (2005) 1702–1708. https://doi.org/10.1016/j.surfcoat.2005.08.088.

[60] K. Khlifi, A.B.C. Larbi, Mechanical properties and adhesion of TiN monolayer and TiN/TiAlN nanolayer coatings, J. Adhes. Sci. Technol. 28 (2014) 85–96. https://doi.org/10.1080/01694243.2013.827094.

[61] S.J. Bull, Failure modes in scratch adhesion testing, Surf. Coatings Technol. 50 (1991) 25–32. https://doi.org/10.1016/0257-8972(91)90188-3.

[62] A.C. Hee, Y. Zhao, S.S. Jamali, P.J. Martin, A. Bendavid, H. Peng, X. Cheng, Corrosion behaviour and microstructure of tantalum film on Ti6Al4V substrate by filtered cathodic vacuum arc deposition, Thin Solid Films. 636 (2017) 54–62. https://doi.org/10.1016/j.tsf.2017.05.030.

[63] T. Kokubo, H.M. Kim, M. Kawashita, Novel bioactive materials with different mechanical properties, Biomaterials. 24 (2003) 2161–2175. https://doi.org/10.1016/S0142-9612(03)00044-9.

[64] R.A. Abdelrahim, N.A. Badr, K. Baroudi, The effect of plasma surface treatment on the bioactivity of titanium implant materials (in vitro), J. Int. Soc. Prev. Community Dent. 6 (2016) 15–21. https://doi.org/10.4103/2231-0762.171592.

[65] J. Xu, X. ke Bao, T. Fu, Y. Lyu, P. Munroe, Z.H. Xie, In vitro biocompatibility of a nanocrystalline β-Ta2O5 coating for orthopaedic implants, Ceram. Int. 44 (2018) 4660–4675. https://doi.org/10.1016/j.ceramint.2017.12.040.

[66] J. Xu, L. Liu, P. Munroe, Z.H. Xie, Promoting bone-like apatite formation on titanium alloys through nanocrystalline tantalum nitride coatings, J. Mater. Chem. B. 3 (2015) 4082–4094. https://doi.org/10.1039/c5tb00236b.

[67] S. Durdu, Ö.F. Deniz, I. Kutbay, M. Usta, Characterization and formation of hydroxyapatite on Ti6Al4V coated by plasma electrolytic oxidation, J. Alloys Compd. 551 (2013) 422–429. https://doi.org/10.1016/j.jallcom.2012.11.024.

[68] A.C. Ciubotariu, L. Benea, M. Lakatos-Varsanyi, V. Dragan, Electrochemical impedance spectroscopy and corrosion behaviour of Al2O3-Ni nano composite coatings, Electrochim. Acta. 53 (2008) 4557–4563. https://doi.org/10.1016/j.electacta.2008.01.020.

[69] Z. Lei, Q. Zhang, X. Zhu, D. Ma, F. Ma, Z. Song, Y.Q. Fu, Corrosion performance of ZrN/ZrO 2 multilayer coatings deposited on 304 stainless steel using multi-arc ion plating, Appl. Surf. Sci. 431 (2018) 170–176. https://doi.org/10.1016/j.apsusc.2017.06.273.

[70] I.M. Penttinen, A.S. Korhonen, E. Harju, M.A. Turkia, O. Forsén, E.O. Ristolainen, Comparison of the corrosion resistance of TiN and (Ti,Al)N coatings, Surf. Coatings Technol. 50 (1992) 161–168. https://doi.org/10.1016/0257-8972(92)90057-H.

[71] A. Ruden, E. Restrepo-Parra, A.U. Paladines, F. Sequeda, Corrosion resistance of CrN thin films produced by dc magnetron sputtering, Appl. Surf. Sci. 270 (2013) 150–156. https://doi.org/10.1016/j.apsusc.2012.12.148.

[72] P.M. Perillo, Properties of CrN Coating Prepared by Physical Vapour Deposition, Am. J. Mater. Sci. Appl. 3 (2015) 38–43. http://www.openscienceonline.com/journal/ajmsa.

[73] R. Brown, M.N. Alias, R. Fontana, Effect of composition and thickness on corrosion behavior of TiN and ZrN thin films, Surf. Coatings Technol. 62 (1993) 467–473. https://doi.org/10.1016/0257-8972(93)90285-V.

[74] C.H. Lin, J.G. Duh, Electrochemical impedance spectroscopy (EIS) study on corrosion performance of CrAlSiN coated steels in 3.5 wt.% NaCl solution, Surf. Coatings Technol. 204 (2009) 784–787. https://doi.org/10.1016/j.surfcoat.2009.09.059.